Targeting hepatic glutaminase activity to ameliorate hyperglycemia

Russell A. Miller[*,±,1,3], **Yuji Shi**[*,3], **Wenyun Lu**[*,2], **David A. Pirman**[4], **Aditi Jatkar**[3], **Matthew Blatnik**[4], **Hong Wu**[4], **César Cárdenas**[5,6,7,8], **Min Wan**[3], **J. Kevin Foskett**[9,10], **Junyoung O. Park**[2,11], **Yiyi Zhang**[12], **William L Holland**[12], **Joshua D. Rabinowitz**[2], and **Morris J. Birnbaum**[±,1,3,10]

[1]Institute for Diabetes, Obesity, and Metabolism, Perelman School of Medicine, University of Pennsylvania, Philadelphia PA

[2]Chemistry and Integrative Genomics, Princeton University, Princeton NJ

[3]Pfizer Internal Medicine Research Units, Cambridge MA

[4]Pfizer Worldwide Research and Development, Groton CT

[5]Anatomy and Developmental Biology Program, Institute of Biomedical Sciences, University of Chile

[6]Geroscience Center for Brain Health and Metabolism, Santiago, Chile

[7]Buck Institute for Research on Aging, Novato, USA

[8]Department of Chemistry and Biochemistry, University of California, Santa Barbara, California 93106, United States

[9]Department of Physiology, Perelman School of Medicine, University of Pennsylvania, Philadelphia PA

[10]Department of Cell and Developmental Biology, Perelman School of Medicine, University of Pennsylvania, Philadelphia PA

[11]Department of Chemical and Biological Engineering, Princeton University, Princeton NJ

[±]Address correspondence to: Morris J. Birnbaum – morris.birnbaum@pfizer.com, 1 Portland Street, Cambridge MA, 02139, *and* Russell A. Miller – Russell.miller@pfizer.com, 1 Portland Street, Cambridge MA, 02139.
[*]These authors contributed equally

[12]Touchstone Diabetes Center, Department of Internal Medicine, The University of Texas Southwestern Medical Center, Dallas TX

Glucagon levels increase under homeostatic, fasting conditions, promoting the release of glucose from the liver by accelerating the breakdown of glycogen (also known as glycogenolysis), while enhancing gluconeogenic flux, including from an increase in the hepatic consumption of amino acids[1]. In type 2 diabetes, dysregulated glucagon signaling contributes to elevated hepatic glucose output and fasting hyperglycemia that occurs in this condition. Yet the mechanism by which glucagon stimulates gluconeogenesis remains incompletely understood. Contrary to the prevailing belief that glucagon acts primarily on cytoplasmic and nuclear targets, we find a glucagon-dependent stimulation of mitochondrial anaplerotic flux from glutamine that increases the contribution of this amino acid to the carbons of glucose generated during gluconeogenesis. This enhanced glucose production is protein kinase A (PKA)-dependent and is associated with glucagon-stimulated calcium release from the endoplasmic reticulum, activation of mitochondrial α-ketoglutarate dehydrogenase, and increased glutaminolysis. Mice with reduced levels of hepatic glutaminase 2 (GLS2), the enzyme that catalyzes the first step in glutamine metabolism, show lower glucagon-stimulated glutamine-to-glucose flux *in vivo*, and GLS2 knockout results in higher fasting plasma glucagon and glutamine with lower fasting blood glucose levels in insulin-resistant conditions. As found in Genome Wide Association Studies (GWAS), human genetic variation in the region of GLS2 is associated with higher fasting plasma glucose[2,3]; here we show in human cryopreserved primary hepatocytes in vitro that these natural gain-of-function missense mutations in GLS2 result in higher glutaminolysis and glucose production. These data emphasize the importance of gluconeogenesis from glutamine, particularly in pathological states of increased glucagon signaling, while suggesting a possible new therapeutic avenue to treat hyperglycemia.

Nearly 50 years ago it was observed that glucagon-dependent increases in glucose production in perfused rat liver were associated with immediate changes in protein phosphorylation resulting from enhanced cAMP production[4]. Subsequent work identified PKA-mediated phosphorylation events that work in concert to increase gluconeogenesis and glycogenolysis in response to glucagon[1]. While these actions of glucagon are the key drivers of acute stimulation of hepatic glucose production, during longer fasting the glucagon-stimulated uptake and oxidation of amino acids, in concert with their release from skeletal muscle, provides access to an additional pool of gluconeogenic substrates to further support fasting glucose production and the proper maintenance of systemic glucose levels.

Whereas lactate provides the most significant and well-studied source of carbon for gluconeogenesis, amino acids also contribute to gluconeogenesis, with glutamine potentially important given its role as a physiological nitrogen shuttle[5]. We therefore set out to test the impact of glucagon on the metabolic flux of lactate and glutamine in mouse primary hepatocytes. Hepatocytes isolated from fasted mice were incubated with physiologically relevant ratios of lactate and glutamine with only one of the substrates labeled with [13]carbon: [U-^{13}C]lactate:[^{12}C]glutamine or [^{12}C]lactate:[U-^{13}C]glutamine. In both of these conditions glucagon was equally capable of stimulating an increase in glucose production

from the labeled cells after 60 minutes of treatment (Fig. 1a–b). Isotopic distribution of extracellular glucose was analyzed under these conditions and revealed a marked change in the distribution and absolute levels of isotopomers (Fig. 1a–d). Glucagon treatment resulted in a reduction in the fractional contribution of lactate to glucose and an increase in the input of glutamine (Fig. 1c–d). Intracellular metabolites were also assessed over time in the same experiments to map the metabolic flux underlying the switch in gluconeogenic substrates. In the presence of [U-^{13}C]lactate and [^{12}C]glutamine, key TCA metabolites showed a modest glucagon-stimulated decrease in labeling (Fig. 1e–f and Supplemental Figure 1). In contrast, cells incubated in [^{12}C]lactate and [U-^{13}C]glutamine showed a large increase in the contribution of glutamine carbon to intracellular metabolites following glucagon treatment (Fig. 1g–h and Supplemental Figure 2). After glucagon stimulation there was robust generation of [$^{13}C_5$]α-ketoglutarate, leading to an approximately 40% enrichment at steady state (Fig. 1g and Supplemental Figure 2).

To obtain a quantitative view of underlying metabolic changes, we modeled the metabolic flux distribution that is consistent with the observed ^{13}C-labeling data (Fig. 1i–j, Supplemental Figure 3, and Supplemental Table 1). Glucagon stimulated pyruvate carboxylase flux about 1.5-fold, while glutaminolysis was increased about 3-fold, resulting in a shift from lactate to glutamine as gluconeogenic substrates. In summary, these results demonstrate that, while lactate is the greater source of gluconeogenic substrate under basal and hormone-stimulated conditions, the contribution of glutamine carbons to newly synthesized glucose is more greatly enriched in response to glucagon stimulation.

When primary hepatocytes were provided with lactate as the sole gluconeogenic substrate, glucagon elicited a reduction of α-ketoglutarate levels within one minute that persisted for the duration of the 1 hour experiment (Fig. 2a). Intracellular glutamate levels also fell in response to glucagon (Fig. 2b). In contrast, glucagon only transiently reduced α-ketoglutarate levels in the presence of [^{12}C]lactate and [U-^{13}C]glutamine, presumably due to the contribution of glutamine to anaplerosis (Fig. 2c). The recovery of α-ketoglutarate levels was accompanied by increased fraction of [$^{13}C_5$] α-ketoglutarate, indicating increased formation of α-ketoglutarate from glutamine (Fig. 2d). In the presence of glutamine, glucagon no longer caused a reduction of intracellular glutamate but instead increased the levels after 10 minutes (Fig. 2e–f). Glucagon treatment did not result in changes in the levels of intracellular glutamine (Supplemental Figure 4).

The glucagon-dependent decrease in α-ketoglutarate in primary hepatocytes was confirmed using a biochemical assay; moreover, glucagon administered *in vivo* elicited a reduction in hepatic α-ketoglutarate (Supplemental Figure 5a–b). Consistent with the increased α-ketoglutarate flux, mitochondria isolated from glucagon-treated cells displayed activation of α-ketoglutarate dehydrogenase (AKGDH) (Supplemental Figure 5c). These data suggest that an immediate effect of glucagon in the liver is the stimulation of gluconeogenesis from glutamine, at least in part through activation of AKGDH. In addition to glucagon, dibutyryl-cAMP effectively reduced α-ketoglutarate levels in primary hepatocytes indicating that like of the effects of glucagon, stimulation of AKGDH was mediated by activation of adenylate cyclase and increases in intracellular cAMP (Supplemental Figure 5a).

To test whether PKA was required for the effects of glucagon mice were infected with a recombinant adeno-associated virus vector that contained a hepatocyte-specific promoter controlling the expression of a mutant PKA regulatory subunit (PKA-RIα) that was unable to bind cAMP and thus behaved like a dominant inhibitor (AAV-PKA-DN)[6,7]. While glucagon was able to increase glucose output and lower α-ketoglutarate in control cells, glucagon failed to stimulate glucose output and reduce cellular α-ketoglutarate in AAV-PKA-DN expressing cells (Fig. 2g–h). In these same cells, glucagon-dependent phosphorylation of the PKA target proteins PFK/FBPase 1, inositol 1,4,5, trisphosphate receptor (IP3R), and CREB was significantly attenuated by AAV-PKA-DN (Supplemental Figure 5d). Pharmacological inhibition of PKA with H89 also blocked the changes in glucose output and α-ketoglutarate in response to glucagon (Supplemental Figure 5e–f). These data show that, like the cytoplasmic and nuclear actions of glucagon, hormone-dependent alterations in mitochondrial metabolism require activation of PKA.

We investigated Ca^{++} as a potential mediator of the actions of glucagon on TCA cycle flux. In primary mouse hepatocytes, glucagon elicited an increase in intracellular Ca^{++} concentration derived from intracellular stores (Supplemental Figure 5g). PKA phosphorylates the IP_3R, an endoplasmic reticulum Ca^{++} release channel, enhancing its sensitivity to IP_3 (ref. 8) IP_3R phosphorylation was absent in cells infected with AAV-PKA-DN, indicating its dependence on the cAMP-PKA signaling pathway (Supplemental Figure 5d).

The α-1 adrenergic receptor agonist phenylephrine activates phospholipase-C and causes an IP_3-dependent increase in intracellular Ca^{++} concentration[8]. Unlike glucagon, phenylephrine did not stimulate phosphorylation of PKA substrates PFK/FBPase 1, CREB, or IP_3R (Supplemental Figure 5d). Phenylephrine treatment resulted in only modest impact on glucose output but equivalent reductions in α-ketoglutarate as compared to glucagon; expression of AAV-PKA-DN had no impact on the effects of phenylephrine (Fig. 2g–h). In primary hepatocytes incubated with [U-^{13}C]glutamine and [^{12}C]lactate, glucagon and phenylephrine enhanced similarly the fractional labeling of extracellular glucose and intracellular metabolites (Supplemental figure 5h–l). In contrast, glucagon more strongly stimulated glucose synthesis and the total amount of ^{13}C-incorporation from glutamine into glucose (Supplemental Figure 5h). These data provide evidence that both glucagon and phenylephrine use Ca^{++} as an intracellular signal to enhance AKGDH activity, thereby biasing substrate selection for gluconeogenesis towards glutamine.

We next tested whether engineered reduction in hepatic glutaminase by knockdown of hepatic *GLS2* gene expression is sufficient to alter systemic glucose homeostasis in mice *in vivo*. Infection of mice by AAV2/8 virus that expressed an shRNA targeting the *GLS2* gene (AAV-GLS2-sh) lowered GLS2 protein levels (Fig. 3a). We performed *in vivo* infusion studies with [U-^{13}C]glutamine and either saline or glucagon, then monitored hepatic metabolites by mass spectrometry. As was observed in primary hepatocytes, in the mice infected with the negative control AAV-GFP, glucagon caused a ~3 fold increase in the contribution of glutamine to glucose that was absent in mice infected with the AAV-GLS2-sh virus (Fig. 3b). Glucagon also caused a glutaminase-dependent increase in the fractional labeling of glycerol-3-phosphate in control liver, though the numerical increase failed to

achieve statistical significance (Fig. 3c). The TCA cycle metabolites glutamate and malate exhibited reduced labeling at baseline in the AAV-GLS2-sh-treated mice, indicating reduced glutamine to glutamate flux, but their labeling in control and glutaminase knockdown liver was unaffected by glucagon (Supplemental Figure 6a–b). This unexpected finding might be the result of the restricted periportal expression of GLS2 and glutamine-derived gluconeogenesis[9].

We next examined the role of GLS2 knockdown on systemic glucose homeostasis. Despite a reduction in contribution of glutamine to hepatic glucose in the AAV-GLS2-sh-injected animals, there was no significant lowering of blood glucose compared to control animals (Fig. 3d). However, the concentration of insulin was significantly reduced in plasma form AAV-GLS2-sh-injected mice, indicating enhanced insulin sensitivity (Fig. 3e). Consistent with this notion, intracellular markers of insulin action, IRβ and Akt phosphorylation, were also lower in the livers of AAV-GLS2-sh-infected mice (Fig. 3a). These data indicate that despite the lack of change in glucose levels following knockdown of GLS2, the lesser requirement of insulin to maintain normoglycemia indicated enhanced insulin sensitivity.

To better understand the contribution of GLS2 to glucose homeostasis, we generated germline GLS2 knockout (KO) mice; the absence of GLS2 protein in the hepatocytes was confirmed by western blot (Supplemental Figure 6c). Primary hepatocytes were isolated from fasted GLS2 wild-type (WT) or GLS2-KO mice and subjected to glucose output assays (Fig. 3f). With physiological levels of glutamine as the sole substrate at 1mM, glucagon stimulated glucose production in GLS2-WT but not KO hepatocytes. In contrast, glucose production from lactate was similar in GLS2-WT and GLS2-KO primary hepatocytes. When both lactate and glutamine were provided as substrates, GLS2-KO primary hepatocytes produced less glucose at baseline and were less responsive to glucagon. These data indicate that GLS2 is an essential enzyme for glucagon-induced flux from glutamine to glucose in primary hepatocytes.

We next examined whether systemic glucose homeostasis was altered by loss of GLS2. GLS2-KO mice showed a reduction in blood glucose after overnight fasting but no change 4h after refeeding (Fig. 3g). Fasting plasma glucagon (Fig. 3h) and glutamine levels (Fig. 3i) were significantly higher in GLS2-KO mice, with no change in insulin level (Fig. 3j), indicating glucagon resistance in the liver. To investigate the underlying mechanism responsible for the elevation of glucagon in GLS2-KO mice, we measured α-cell and β-cell mass in pancreatic islets from fasted mice (Fig. 3k). Pancreatic islets from GLS2-KO mice demonstrated α-cell hyperplasia (Fig. 3l), with no significant changes in β-cell mass (Fig. 3m).

To understand the importance of GLS2 in a disease setting, mice were challenged with a 60% high fat diet. After 17 weeks on this diet, GLS2 KO mice exhibited a significant reduction in fasting glucose levels without significant changes in body weight, insulin, or glucagon (Fig. 3n–q). Taken together, these data support an important function of GLS2 mediating the glucose output in fasting in response to glucagon.

Common genetic variants in a locus that includes the human liver glutaminase gene (*GLS2*) are associated with BMI-adjusted fasting plasma glucose and plasma glutamine levels[2,3]. A common variation resulting in replacement of leucine 581 by proline (L581P) is the polymorphism most highly associated with higher fasting plasma glucose and lower plasma glutamine. To determine whether this association is the result of higher glutaminase flux, we genotyped cryopreserved human hepatocytes and identified 6 lots heterozygous for the L581P allele (L581L/P) and 6 lots homozygous for the major 581L allele (L581L/L) that were matched for available donor characteristics. Hepatocytes from L581L/P donors exhibited greater glucose production than control hepatocytes under basal conditions or after treatment with glucagon (Figure 4a). Incubation of *GLS2* L581L/P hepatocytes with [U-^{13}C]glutamine and unlabeled lactate and pyruvate resulted in both more rapid labeling and greater enrichment at steady state than homozygous L581L/L hepatocytes of multiple TCA and gluconeogenic intermediates (Figure 4b–h). This increased labeling of TCA intermediates occurred despite equivalent fractional enrichment in intracellular glutamine, implicating a higher rate of glutamine to glutamate flux in the L581L/P hepatocytes. To confirm that *GLS2*(L581P) is a gain-of-function mutation, we over-expressed either GLS2(WT) or GLS2(L581P) in immortalized human hepatocytes and measured intracellular glutamate levels. Consistent with previous reports[10,11], exogenous GLS2(WT) expression significantly increased intracellular glutamate, while GLS2(L581P) further elevated intracellular glutamate level (Figure 4i). These data, in combination with the higher blood glucose levels in individuals with GLS2 L581P variants, provide clear evidence that the contribution of glutaminolysis to gluconeogenesis is physiologically significant and of sufficient magnitude to impact glucose homeostasis in humans.

In addition to the absolute rate of gluconeogenesis, the supply of major gluconeogenic substrates is a critical factor necessary for sustained gluconeogenesis during fasting. Accelerated glutamine turnover has been observed in conditions associated with elevated glucagon levels *in vivo*, including fasting and exercise, physiological states that are also associated with a reduction in serum glutamine levels[12–16]. Preferential utilization of glutamine under these conditions is likely related to the need for a stable pool of hepatic glucose precursors and the essential transfer of nitrogen from muscle amino acids to liver for conversion to urea and excretion[12,17,18]. In this report we have demonstrated a molecular mechanism by which glucagon biases hepatic metabolism towards the utilization of glutamine. Unlike glucagon's effects on cytoplasmic enzyme activity, its mitochondrial actions serve to not only increase gluconeogenesis but also to modify substrate selection. While lactate accounted for the majority of the carbons destined for synthesis of glucose under both basal and hormone-stimulated conditions, glucagon stimulated a disproportionately greater increase in gluconeogenesis from glutamine. In this manner, glutaminolysis is responsible for the majority of the hormone-dependent increase in gluconeogenesis and probably contributes significantly to the rapid surge in mitochondrial respiration that has been long-recognized as an important component of glucagon's actions[19,20]. Thus, the glucagon-dependent shift to glutamine utilization is critical for the liver and organism during fasting states.

The kidney is also capable of glutamine-derived gluconeogenesis[21]. The fractional contribution of glutamine to renal gluconeogenesis is greater than that in the liver[13].

However, the impact of glucagon on glutamine-derived gluconeogenesis is restricted to the liver; increases in glucagon are capable of augmenting hepatic glutamine-derived gluconeogenic rate to a level that surpasses the rate of glutamine-derived renal gluconeogenesis[13]. Therefore, glucagon signaling and systemic tone result not only in a change in hepatic gluconeogenic substrate selection but also in a change in the major sites of systemic consumption of this amino acid.

There have been previous indications that glucagon regulates mitochondrial metabolism. Glucagon elicits a rapid and significant enhancement of mitochondrial Ca^{++} uptake, driven by glucagon-stimulated increases in cytoplasmic Ca^{++} concentration due to release from intracellular stores[22–25] and Ca^{++} influx across the plasma membrane[26,27]. The former has been proposed to be due to PKA-mediated phosphorylation of the IP_3R (ref. 8). One consequence of activating IP_3R-mediated Ca^{++} release is the efficient transfer of Ca^{++} into mitochondria, where it activates dehydrogenases and stimulates TCA cycle activity[28]. In hepatocytes, glucagon reduces cellular α-ketoglutarate and activates α-ketoglutarate dehydrogenase[29,30]. In the current study, we have confirmed and extended these observations and can now integrate them into a coherent and quantitative model of how glucagon rapidly activates preferential flux from glutamine into glucose (Figure 4j). Moreover, we have provided the first genetic evidence that this pathway is quantitatively significant in human liver. We propose that PKA-dependent phosphorylation of the IP_3R leads to Ca^{++} release from the ER, raising mitochondrial matrix Ca^{++} concentration with consequent α-ketoglutarate dehydrogenase activation, stimulation of mitochondrial respiration and reduction of the levels of α-ketoglutarate. The ability of both glucagon and phenylephrine to promote the anaplerotic entry of substrate into the TCA cycle as α-ketoglutarate emphasizes the critical role of Ca^{++} as a signaling intermediate. Glucagon also activates glutaminolysis, resulting in increased cellular glutamate content and ^{13}C enrichment from glutamine in both mouse and human hepatocytes; however the precise mechanisms for this remain unclear[31,32]. Glucagon has also been shown to increase the rate of glutamine transport in conjunction with increased glutaminase activity[34]; our work does not formally distinguish between these two points of flux control, but our data showing no increase in hepatocyte glutamine levels following glucagon treatment despite increased cellular glutamate would suggest glutamine transport is a minor contributor.

The absence of GLS2 protein completely blocked the flux from glutamine to glucose in primary hepatocytes. Consistent with glutamine serving as a major glucagon-stimulated gluconeogenic substrate, GLS2-KOhepatocytes had minimal glucagon stimulation when a physiological mixture of lactate and glutamine were used as substrates. Glutamine flux appears to represent a quantitatively significant contributor to systemic glucose production in mice and humans, as indicated by plasma glucose increase elicited by a gain-of-function polymorphism in the *GLS2* gene and the removal of GLS2 in mice. It is likely that the glucagon-dependent activation of hepatic glutaminolysis is an important component of both normal variation in circulating metabolites and the pathophysiology of T2DM. These studies raise the intriguing possibility that *GLS2* could represent a novel, genetically validated T2DM target for improvement of glucose homeostasis.

Online Materials and Methods

Materials

AAV-PKA-DN virus was constructed by cloning a cDNA encoding the dominant inhibitory PKA-RIab into an AAV plasmid that contained a hepatocyte specific promoter (Thyroid Binding Globulin, TBG)[33]. shRNA targeting the mouse *GLS2* gene was created the 21 bp sequence GCGTATTTGAGGATGCCAAAG after the U6 promoter in an AAV vector. AAV virus was produced at the University of Pennsylvania Vector Core. Stable isotope substrates were purchases from Cambridge Isotopes. All other chemicals were purchased from Sigma Aldrich. Antibodies specific for phosphorylated (Serine 1756) and total IP$_3$R, phosphorylated (Serine 133) and total CREB, phosphorylated (Tyr1150/1151) and total Insulin Receptor β, phosphorylated (Serine 473) and total Akt, total GAPDH and β-actin antibodies were purchased from Cell Signaling Technology. Total PFKFB1 antibody was purchased from AbCam (ab71625). Total GLS2 antibody was purchased from Sigma. The phosphorylated (Serine 33) PFKFB1 antibody was produced by Cell Signaling Technology[6]. Cryopreserved human hepatocytes were purchased from BD Biosciences. Immortalized human hepatocytes were purchased from ATCC. Lentivirus for GLS2 over-expression was constructed by cloning cDNA expressing either GLS2-WT or GLS2(L581P) into pCDH expression lenti-vector from system biosciences. Amplex Red glutamic acid/glutamate oxidase assay kit was purchased from ThermoFisher Scientific. Ultra sensitive mouse insulin Elisa kit was from Crystal Chem. Glucagon 10µl Elisa kit was purchased from Mercodia. Glutamine Assay kit (KA1627) was from Abnova.

GLS2 knockout mice

Mice with constitutive knock-out of the Gls2 gene via Cas9-mediated gene editing were created and provided by Taconic Biosciences. The targeting strategy was achieved through co-injection of the Cas9 mRNA, the proximal and distal sgRNAs into C57BL/6NTac zygotes, resulting in deletion of exons 2 to 7 of Gls2 gene. The off-target analysis was based on the GRCm38/mm10 assembly. The potential non-intergenic off-target sites analysis was performed in the G1 generation and none of the off-target sites were found.

In vivo and primary hepatocyte glucose output studies

All animal studies followed ethical guidelines and were approved by University of Pennsylvania or Pfizer IACUC. In vivo animal studies were performed in 12 week old male C57bl/6 mice and were not randomized or blinded. Primary hepatocytes were isolated from male C57bl/6 mice between 12–18 weeks of age by the two-step collagenase perfusion method using Liver Digest reagents from Invitrogen[34]. After isolation, cells were plated in M199 media with 10% FBS for 3 hours in multiwell plates precoated with collagen I. After cells attached to the plates, they were washed with glucose output media (GOM) (118 mM NaCl, 4.7 mM KCl, 1.2 mM MgSO$_4$, 1.2 mM KH$_2$PO$_4$, 1.2 mM CaCl$_2$, 20 mM NaCO3, 25 mM HEPES pH 7.4, and 0.025% BSA), and incubated in fresh GOM for 1 hour. GOM media was replaced with fresh, pre-warmed GOM media and cellular treatments initiated. For glucose output studies, the cells were given the indicated gluconeogenic substrates and extracellular glucose was assayed after 1 hour using a hexokinase-based glucose assay kit (Sigma Aldrich), and data were normalized to total cellular protein. Glucose production

assays to quantify rates of lactate and glutamine consumption and pyruvate production for modeling purposes were performed by treating cells as above in glucose production assays with 5 mM [$^{12}C_3$]lactate and 2.5 mM [$^{12}C_5$]glutamine. At 30 minutes and 1 hour media was removed, centrifuged to remove loose cells, and an equal volume of methanol containing 5 mM [$^{13}C_3$]lactate, 2.5 mM [$^{13}C_5$]glutamine, 0.5 mM [$^{13}C_1$]pyruvate, and 0.5 mM [$^{13}C_6$]glucose. After removal of media cells were lysed and protein measured. Media-methanol mixtures were analyzed by mass spectrometry and rates of metabolite production and consumption measured.

Glutamine infusion studies

12 week old C57bl/6 mice were purchased from Jackson Laboratories with an indwelling jugular vein catheter. 4 days after arrival animals were infected with AAV-GFP or AAV-GLS2-sh at a dose of 10e11 viral genomes per animal. 2 weeks after infection mice were fasted at 6AM, lines were flushed with heparin in saline, and hooked up to infusion pumps. After 4 hours of fasting pumps began to infuse animals with 0.25 mmol/kg/hr of [U-^{13}C]glutamine for 1 hour. After 1 hour pump solutions were switched to include either 0.25 mmol/kg/hr of [U-^{13}C]glutamine or 0.25 mmol/kg/hr of [U-^{13}C]glutamine with the addition of 1 mg/kg/hr of glucagon. After 1 hour of infusion animals were anesthetized with pentobarbital, liver tissue was collected and rapidly frozen in liquid nitrogen, and terminal blood was collected by cardiac stick.

Mass spectrometry

Primary hepatocytes were given the indicated gluconeogenic substrates and reactions were stopped by rapidly removing culture media and adding to the cells 80% methanol pre-cooled in dry ice. Cellular debris was removed by centrifugation and samples dried by speedvac. The dried cell extracts were re-dissolved in 200 μL HPLC-grade water, and analyzed via reverse-phase ion-pairing chromatography coupled to an Exactive orbitrap mass spectrometer (ThermoFisher Scientific, San Jose, CA). The mass spectrometer was operated in negative ion mode with a scan rate of 1 Hz and resolving power of 100,000, scanning range being *m/z* 85–1000. The LC method has been described before[35], using a Synergy Hydro-RP column (100 mm × 2 mm, 2.5 μm particle size, Phenomenex, Torrance, CA) with a flow rate of 200 μL/min. The LC gradient was 0 min, 0% B; 2.5 min, 0% B; 5 min, 20% B; 7.5 min, 20% B; 13 min, 55% B; 15.5 min, 95% B; 18.5 min, 95% B; 19 min, 0% B; 25 min, 0% B. Solvent A is 97:3 water–methanol with 10 mM tributylamine and 15 mM acetic acid; solvent B is methanol. Other LC parameters were autosampler temperature 5°C, injection volume 10 μL, and column temperature 25 °C.

Data analyses were performed using MAVEN software[36], which performs both peak alignment and quantitation (for both labeled and unlabeled forms) and allows user validation by extracted ion chromatogram visualization. All peak identities were confirmed by exact mass and retention time match to authenticated metabolite standard. Ion signals were further processed to correct for the natural isotope abundance of the unlabeled glucose and trace unlabeled impurity in the labeled substrates.

Metabolic flux analysis

Mass isotopomer distributions of intracellular and extracellular metabolites were obtained via LC-MS when cells were incubated with $[^{13}C_5]$glutamine or $[^{13}C_3]$lactate. Intracellular metabolites, glucose 6-phosphate, glycerol 3-phosphate (proxy for dihydroxyacetone phosphate), 3-phosphoglycerate, phosphoenolpyruvate, pyruvate, acetyl-CoA, α-ketoglutarate, succinate, malate, aspartate (proxy for cytosolic oxaloacetate), and glutamate, were included in the flux calculation. In addition, measured lactate and glutamine uptake as well as glucose and pyruvate secretion rates were input. Lactate exchange rate, that is, the rate at which $[^{13}C]$lactate appears in the medium when $[^{13}C]$glutamine and $[^{12}C]$lactate were used as carbon sources, was measured. A cumomer network encompassing TCA cycle, anaplerotic and gluconeogenic reactions was generated using 13CFLUX2 (http://www.13cflux.net)[37,38]. The flux distributions that minimize the variance-weighted sum of squared residuals between measured and computed mass isotopomer distributions were obtained by iteratively invoking the interior-point optimization algorithm in Matlab. Subsequently, 95% confidence intervals around the optimal fluxes were calculated[39].

α-ketoglutarate assays

Primary hepatocytes were incubated with 5 mM lactate for 30 minutes and then treated as indicated. Reactions were stopped by removing the culture media and α-ketoglutarate was extracted with the addition of 80% methanol. Cellular debris was removed by centrifugation and samples dried by speedvac. α-Ketoglutarate and pyruvate were quantified in a coupled glutamic-transaminase and pyruvate oxidase reactions in the presence of horse radish peroxidase and amplex red[40]. Briefly, reactions containing 100 mM KPO_4 pH 6.8, 1 mM EDTA, 1 mM $MgCl_2$, 10 μM FAD, 200 μM TPP, 20 mM Alanine, 25 μM Amplex Red, 0.5 units/mL Horseradish peroxidase, 0.2 units/mL Pyruvate Oxidase, and +/− 0.2 units/mL of Glutamic-Pyruvic Transaminase were incubated for 30 minutes with samples or α-ketoglutarate standards. Amplex red fluorescence was quantified with excitation by 535 nM light, detecting emission of 587 nM light, and values from samples lacking transaminase were subtracted from transaminase containing samples.

α-ketoglutarate dehydrogenase assays

For α-ketoglutarate dehydrogenase assays, mitochondria were isolated by differential centrifugation from primary hepatocytes treated as indicated[41]. Assay buffer included 20 mM HEPES pH 7.4, 1 mM $MgCl_2$, 100 μM CoA, 2.5 mM NAD^+, 0.01% rotenone, 2 mM KCN, 1 mM DTT, +/− 50 μM α-ketoglutarate. Assays were started by addition of mitochondria and NADH production was monitored by the absorbance at 340 nM.

Calcium measurements

Freshly isolated primary hepatocytes from wild type C57Bl/6 mice were plated on collagen-coated coverslips, allow to attach for 3 hours, and loaded with Fura-2 dye. Images were acquired with a continuous flow of media for rapid switching of treatment conditions. Fluorescent ratios were compared to standard curves to estimate total cytoplasmic calcium levels.

Human hepatocyte genotyping

41 cryopreserved human hepatocyte lots were purchased from BD Biosciences (Franklin Lakes, NJ, USA) and Life Technologies (Grand Island, NY). Genomic DNA was extracted using the QIAamp DNA Micro Kit (Qiagen, Valencia, CA) in accordance with the manufacturer's instructions. DNA was resuspended to a concentration of 5–10 ng/uL for subsequent genotyping analysis. Genotyping of rs2657879 (c.1742T>C) was performed following a 411 bp genomic amplification using the primers rs2657879F (TTTGCCAAGGACAGGTGAGG) and rs2657879r (CTTGGTCCCCACTGAAGCAG). The PCR product was sent to Beckman Coulter Genomics for direct sequencing using the primer rs2657879seq (TTTGCCAAGGACAGGTGAGG).

Cryopreserved human hepatocyte culture

Cryopreserved human hepatocytes were thawed in High Viability CryoHepatocyte Recovery Medium (Cat#454560, BD Biosciences, St Paul, MN, USA). Nonviable cells were removed following the cell vendor's protocol prior to cell plating. Viable cells were plated onto collagen coated 48 well plates (150,000 cells/well) in Invitrogen plating media (Celsis IVT Z99029, Bioreclemation IVT, Baltimore MD, USA) and were allowed to attach for 6 hours. After attachment media was replaced with fresh low glucose DMEM media plus 10% FBS and 1 μM glucagon (Cat# G3157, Sigma Aldrich, St Louis, MO, USA). The following day cells were incubated in Krebs buffer for 1 hour without gluconeogenic substrates. At time 0 the media was switched to media with 5 mM $[^{12}C_3]$lactate, 0.5 mM $[^{12}C_3]$pyruvate, and 2.5 mM $[^{13}C_5]$glutamine. Cells were incubated for 1, 5, 15, 60, or 180 minutes, washed in warm PBS, and lysed with the addition of cold 80% methanol. Cells were scraped and cellular debris pelleted through centrifugation. Supernatants were collected, dried under vacuum, and reconstituted in 100 100 μL of 0.1% formic acid prior to LC-HRAMS analysis

Immunofluorescence of pancreatic islets

Immunofluorescent staining for insulin and glucagon were performed as previously described on multiple, non-adjacent 5μM sections no closer than 50 μM apart[42]. Glucagon antibody was from Abcam (Cat# 10988, 1:1000 Cambridge, MA) and insulin antibody from dako (Cat# A0564, 1:500; Dako, Carpinteria, CA). Images were collected using a BZ-X710 fluorescence microscope (Keyence, Elmwood Park, NY).

LC-HRAMS analysis and workflow

Analysis of glutamine and its cellular metabolites were conducted by injecting a 10 mL sample aliquot onto an Imtakt UK-Phenyl (2.1 mm × 150 mm) column (Imtakt USA, Philadelphia, PA, USA) using a Waters Acquity UPLC system (Waters Corp., Milford, MA, USA) coupled to a Thermo Q-Exactive (Thermo Corp., San Jose, CA, USA) mass spectrometer. Analytes were chromatographically resolved using a linear gradient from 0% to 50% B, or acetonitrile containing 0.3% formic acid, over three minutes at 500 μL min^{-1} with a column temperature of 40 °C. Mobile phase A composition was 0.1% formic acid. Metabolites were monitored using negative ion electrospray (ESI−) in full scan mode with a resolution of 70,000 calibrated to mass accuracy <2 ppm. Instrument parameters were fixed: the sheath gas was 60 AU, the auxiliary gas 40 AU, sweep gas 2 AU, ESI(−) spray voltage

was −3 kV, the capillary temperature was 320 °C, and the S-lens set at 50 AU. Glutamine flux was determined through measurement of expected ^{13}C-glutaminolysis isotopomers. Cell experiments without the addition of labeled glutamine were used as negative controls to ensure identified labeled metabolites were unique to the samples treated with labeled substrate. Thermo LCQuan (Thermo Corp, San Jose, CA, USA) was used to extract out exact mass, extracted ion chromatograms using a 10 ppm window at the calculated accurate mass for each metabolite and isotopomer. Individual isotopomer percentages were normalized to the total sum of all detected isotopomers after natural isotope correction. Data analysis was performed using Microsoft Excel and plots were generated in Graphpad Prism.

Statistics

All results are expressed as the mean ± SEM. All two group comparisons were deemed statistically significant by unpaired 2 tailed student's t-test if $p<0.05$ or 2-way anova. All experimental values were obtained from the measurement of distinct samples and not repeated measures of the same sample. Experiments were performed multiple times as indicated in the figure legends with representative data presented. Sample sizes were selected based on previous knowledge of the variation in experimental methods and expected effect size observed in previous studies. Variation was similar between groups being compared and exhibited apparent normal distribution.

General methods statements

No samples, mice, or studies were removed from the analyses. Samples were not blinded or randomized in this study, except for the analysis of mass spectrometry samples which were run agnostic of groupings. Tissue culture samples were not evaluated for mycoplasma contamination.

Statement of data availability

All analyses are contained within this manuscript and source data is archived and available upon reasonable request. Uncropped images of western blots can be found in the supplementary information.

Supplementary Material

Refer to Web version on PubMed Central for supplementary material.

Acknowledgments

References

1. Miller RA, Birnbaum MJ. Glucagon: acute actions on hepatic metabolism. Diabetologia. 2016; 59:1376–1381. [PubMed: 27115415]

2. Scott RA, et al. Large-scale association analyses identify new loci influencing glycemic traits and provide insight into the underlying biological pathways. Nat Genet. 2012; 44:991–1005. [PubMed: 22885924]

3. Suhre K, et al. Human metabolic individuality in biomedical and pharmaceutical research. Nature. 2011; 477:54–60. [PubMed: 21886157]

4. Exton JH, Park CR. Control of gluconeogenesis in liver. II. Effects of glucagon, catecholamines, and adenosine 3',5'-monophosphate on gluconeogenesis in the perfused rat liver. J Biol Chem. 1968; 243:4189–4196. [PubMed: 5679958]

5. Young VR, Ajami AM. Glutamine: the emperor or his clothes? J Nutr. 2001; 131:2449S–2459S. discussion 2486S–2447S. [PubMed: 11533293]

6. Miller RA, et al. Biguanides suppress hepatic glucagon signalling by decreasing production of cyclic AMP. Nature. 2013; 494:256–260. [PubMed: 23292513]

7. Titchenell PM, et al. Direct Hepatocyte Insulin Signaling Is Required for Lipogenesis but Is Dispensable for the Suppression of Glucose Production. Cell Metab. 2016; 23:1154–1166. [PubMed: 27238637]

8. Williamson JR, et al. Mechanisms involved in receptor-mediated changes of intracellular Ca2+ in liver. Soc Gen Physiol Ser. 1987; 42:93–116. [PubMed: 2850613]

9. Watford M, Smith EM. Distribution of hepatic glutaminase activity and mRNA in perivenous and periportal rat hepatocytes. Biochem J. 1990; 267:265–267. [PubMed: 1970242]

10. Hu W, et al. Glutaminase 2, a novel p53 target gene regulating energy metabolism and antioxidant function. Proc. Natl. Acad. Sci. U. S. A. 2010; 107:7455–7460. [PubMed: 20378837]

11. Suzuki S, et al. Phosphate-activated glutaminase (GLS2), a p53-inducible regulator of glutamine metabolism and reactive oxygen species. Proc. Natl. Acad. Sci. U. S. A. 2010; 107:7461–7466. [PubMed: 20351271]

12. Krishna MG, et al. Glucagon response to exercise is critical for accelerated hepatic glutamine metabolism and nitrogen disposal. Am J Physiol Endocrinol Metab. 2000; 279:E638–645. [PubMed: 10950833]

13. Stumvoll M, Meyer C, Kreider M, Perriello G, Gerich J. Effects of glucagon on renal and hepatic glutamine gluconeogenesis in normal postabsorptive humans. Metabolism. 1998; 47:1227–1232. [PubMed: 9781626]

14. Battezzati A, Simonson DC, Luzi L, Matthews DE. Glucagon increases glutamine uptake without affecting glutamine release in humans. Metabolism. 1998; 47:713–723. [PubMed: 9627372]

15. Hankard RG, Haymond MW, Darmaun D. Role of glutamine as a glucose precursor in fasting humans. Diabetes. 1997; 46:1535–1541. [PubMed: 9313746]

16. Stumvoll M, et al. Glutamine and alanine metabolism in NIDDM. Diabetes. 1996; 45:863–868. [PubMed: 8666134]

17. Perriello G, et al. Estimation of glucose-alanine-lactate-glutamine cycles in postabsorptive humans: role of skeletal muscle. Am J Physiol. 1995; 269:E443–450. [PubMed: 7573421]

18. Nurjhan N, et al. Glutamine: a major gluconeogenic precursor and vehicle for interorgan carbon transport in man. J Clin Invest. 1995; 95:272–277. [PubMed: 7814625]

19. Halestrap AP. Stimulation of the respiratory chain of rat liver mitochondria between cytochrome c1 and cytochrome c by glucagon treatment of rats. Biochem J. 1978; 172:399–405. [PubMed: 210759]

20. Yamazaki RK. Glucagon stimulation of mitochondrial respiration. The Journal of biological chemistry. 1975; 250:7924–7930. [PubMed: 240844]

21. Stumvoll M, Perriello G, Meyer C, Gerich J. Role of glutamine in human carbohydrate metabolism in kidney and other tissues. Kidney Int. 1999; 55:778–792. [PubMed: 10027916]

22. Mauger JP, Claret M, Pietri F, Hilly M. Hormonal regulation of inositol 1,4,5-trisphosphate receptor in rat liver. J Biol Chem. 1989; 264:8821–8826. [PubMed: 2542291]

23. Burgess GM, Bird GS, Obie JF, Putney JW Jr. The mechanism for synergism between phospholipase C- and adenylylcyclase-linked hormones in liver. Cyclic AMP-dependent kinase augments inositol trisphosphate-mediated Ca2+ mobilization without increasing the cellular levels of inositol polyphosphates. J Biol Chem. 1991; 266:4772–4781. [PubMed: 1848225]

24. Bygrave FL, Gamberucci A, Fulceri R, Benedetti A. Evidence that stimulation of plasma-membrane Ca2+ inflow is an early action of glucagon and dibutyryl cyclic AMP in rat hepatocytes. Biochem J. 1993; 292(Pt 1):19–22. [PubMed: 8389124]

25. Fernando KC, Gregory RB, Barritt GJ. Protein kinase A regulates the disposition of Ca2+ which enters the cytoplasmic space through store-activated Ca2+ channels in rat hepatocytes by diverting inflowing Ca2+ to mitochondria. The Biochemical journal. 1998; 330(Pt 3):1179–1187. [PubMed: 9494083]

26. Hughes BP, Barritt GJ. Effects of glucagon and N6O2'-dibutyryladenosine 3':5'-cyclic monophosphate on calcium transport in isolated rat liver mitochondria. Biochem J. 1978; 176:295–304. [PubMed: 215132]

27. Keppens S, Vandenheede JR, De Wulf H. On the role of calcium as second messenger in liver for the hormonally induced activation of glycogen phosphorylase. Biochim Biophys Acta. 1977; 496:448–457. [PubMed: 189844]

28. Denton RM, McCormack JG. Ca2+ transport by mammalian mitochondria and its role in hormone action. Am J Physiol. 1985; 249:E543–554. [PubMed: 2417490]

29. Siess EA, Wieland OH. Glucagon-induced stimulation of 2-oxoglutarate metabolism in mitochondria from rat liver. FEBS Lett. 1978; 93:301–306. [PubMed: 213314]

30. Williamson JR, Browning ET, Thurman RG, Scholz R. Inhibition of glucagon effects in perfused rat liver by (+)decanoylcarnitine. J Biol Chem. 1969; 244:5055–5064. [PubMed: 4309991]

31. Lacey JH, Bradford NM, Joseph SK, McGivan JD. Increased activity of phosphate-dependent glutaminase in liver mitochondria as a result of glucagon treatment of rats. The Biochemical journal. 1981; 194:29–33. [PubMed: 7305982]

32. Joseph SK, McGivan JD. The effect of ammonium chloride and glucagon on the metabolism of glutamine in isolated liver cells from starved rats. Biochim Biophys Acta. 1978; 543:16–28. [PubMed: 708783]

33. Clegg CH, Correll LA, Cadd GG, McKnight GS. Inhibition of intracellular cAMP-dependent protein kinase using mutant genes of the regulatory type I subunit. J Biol Chem. 1987; 262:13111–13119. [PubMed: 2820963]

34. Seglen PO. Preparation of isolated rat liver cells. Methods Cell Biol. 1976; 13:29–83. [PubMed: 177845]

35. Clegg CH, Correll LA, Cadd GG, McKnight GS. Inhibition of intracellular cAMP-dependent protein kinase using mutant genes of the regulatory type I subunit. J Biol Chem. 1987; 262:13111–13119. [PubMed: 2820963]

36. Miller RA, et al. Biguanides suppress hepatic glucagon signalling by decreasing production of cyclic AMP. Nature. 2013; 494:256–260. [PubMed: 23292513]

37. Seglen PO. Preparation of isolated rat liver cells. Methods Cell Biol. 1976; 13:29–83. [PubMed: 177845]

38. Lu W, et al. Metabolomic analysis via reversed-phase ion-pairing liquid chromatography coupled to a stand alone orbitrap mass spectrometer. Anal Chem. 2010; 82:3212–3221. [PubMed: 20349993]

39. Melamud E, Vastag L, Rabinowitz JD. Metabolomic analysis and visualization engine for LC-MS data. Anal Chem. 2010; 82:9818–9826. [PubMed: 21049934]

40. Weitzel M, et al. 13CFLUX2--high-performance software suite for (13)C-metabolic flux analysis. Bioinformatics. 2013; 29:143–145. [PubMed: 23110970]

41. Wiechert W, Mollney M, Isermann N, Wurzel M, de Graaf AA. Bidirectional reaction steps in metabolic networks: III. Explicit solution and analysis of isotopomer labeling systems. Biotechnology and bioengineering. 1999; 66:69–85. [PubMed: 10567066]

42. Antoniewicz MR, Kelleher JK, Stephanopoulos G. Determination of confidence intervals of metabolic fluxes estimated from stable isotope measurements. Metabolic engineering. 2006; 8:324–337. [PubMed: 16631402]

43. Zhu A, Romero R, Petty HR. A sensitive fluorimetric assay for pyruvate. Anal Biochem. 2009; 396:146–151. [PubMed: 19748474]

44. Frezza C, Cipolat S, Scorrano L. Organelle isolation: functional mitochondria from mouse liver, muscle and cultured fibroblasts. Nat Protoc. 2007; 2:287–295. [PubMed: 17406588]

45. Ye R, et al. Adiponectin is essential for lipid homeostasis and survival under insulin deficiency and promotes beta-cell regeneration. eLife. 2014; 3
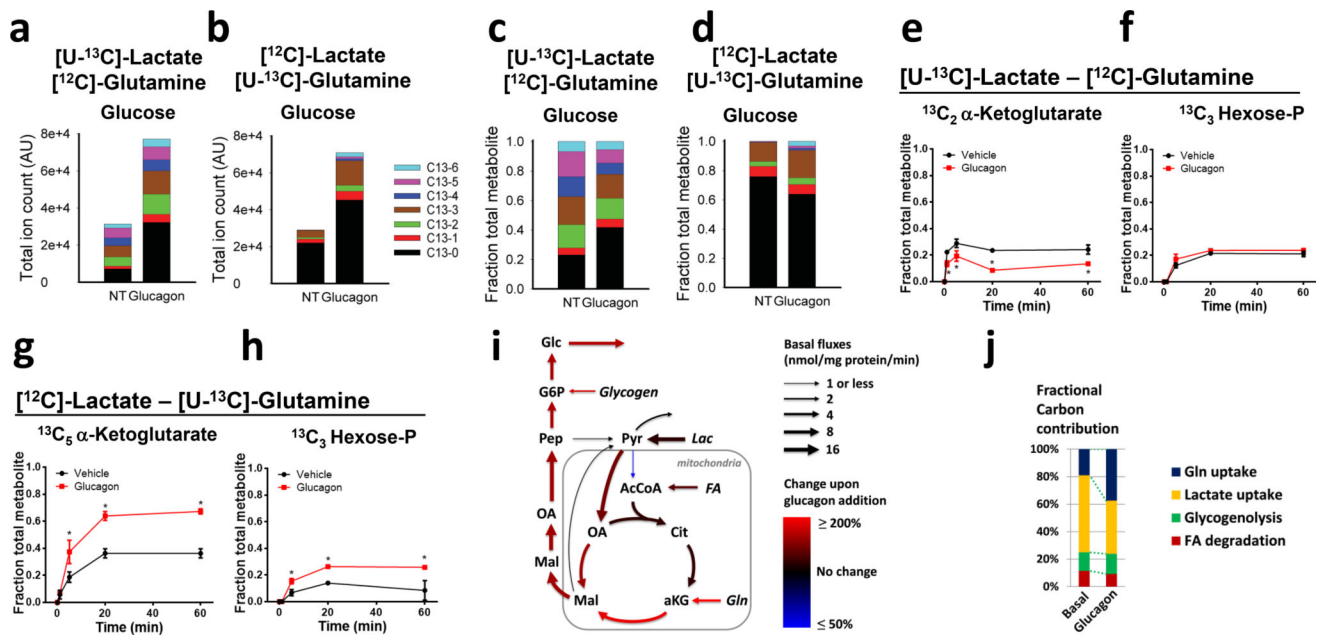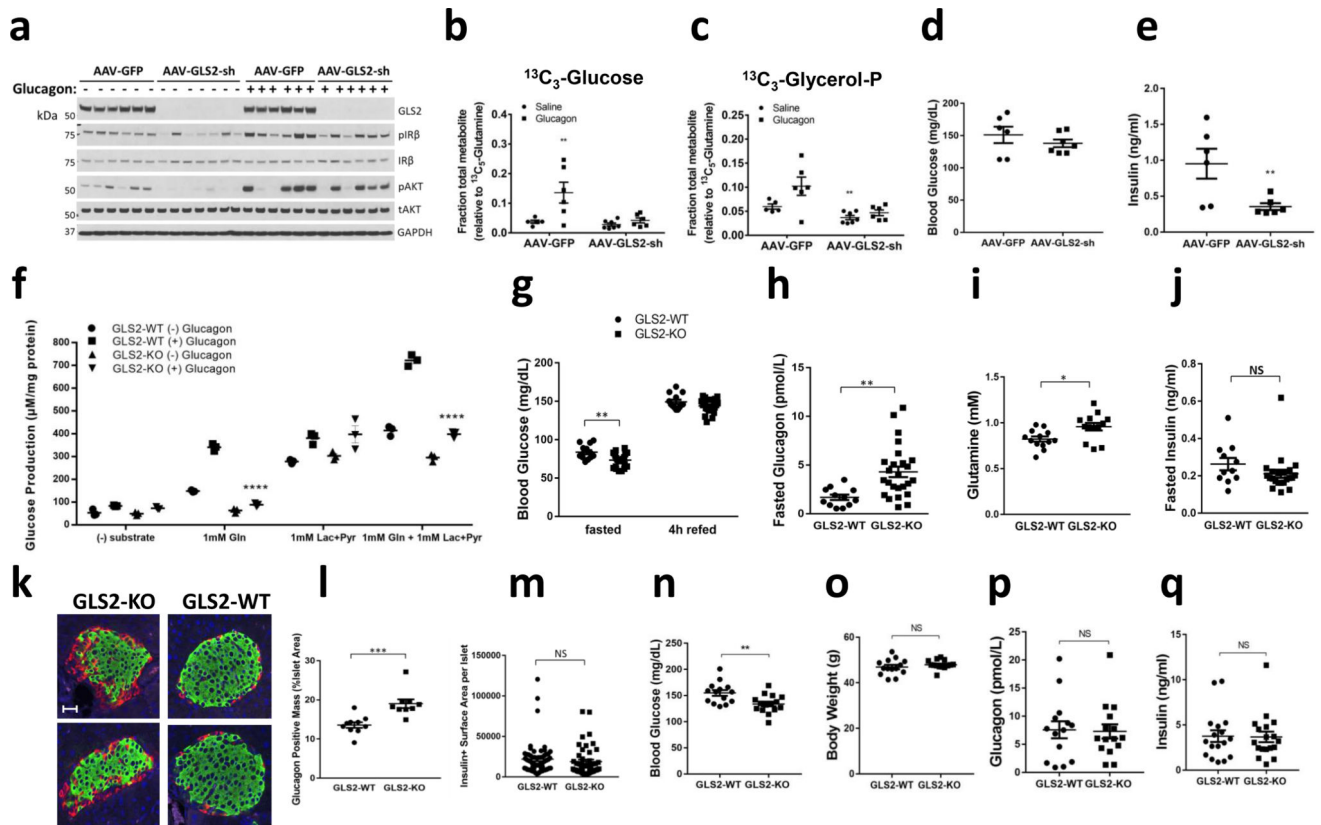
Figure 1.
Glucagon-mediated metabolic flux studies from glutamine in primary hepatocytes. (**a–d**) Absolute amounts of extracellular glucose isotopomers (**a–b**) and relative amounts of extracellular glucose isotopomers (**c–d**) in primary hepatocytes isolated from fasted mice after plating for 4 hours on collagen-coated plates and incubation with 5 mM [U-^{13}C]lactate and 2.5 mM [^{12}C]glutamine or 5 mM [^{12}C]lactate and 2.5 mM [U-^{13}C]glutamine. Cells were treated with glucagon or PBS vehicle (NT). Specific isotopomers of glucose are colored as shown in the legend based on the number of C13 carbons. (**e–h**) Mass spectrometry analysis of intracellular metabolites from primary hepatocytes treated with PBS vehicle or glucagon and incubated with 5 mM [U-^{13}C]lactate and 2.5 mM [^{12}C]glutamine (**e,f**) or 5 mM [^{12}C]lactate and 2.5 mM [U-^{13}C]glutamine (**g,h**). For each metabolite, the most abundant isotopomer derived from the carbon-13 substrate is displayed. Each time point represents the mean and standard error of 3 replicate samples. This experiment was repeated more than three times. (**i**) Graphical representation of fluxes determined by metabolic flux analysis of the data presented in Fig. 1 and Supplemental Fig. 1,2. Net fluxes for the indicated reaction are expressed as nmol/mg protein/min. (**j**) Fractional contribution of carbon as determine from modeling of data presented in Fig. 1 and Supplemental Fig. 1–2. FA: Fatty acids; AcCoA: acetyl-CoA; Cit: Citrate; aKG: α-ketoglutarate; Gln: glutamine; Mal: malate; OA: oxaloacetate; Pep: phosphoenolpyruvate; Pyr: pyruvate; G6P: glucose-6-phosphate; Glc: glucose.
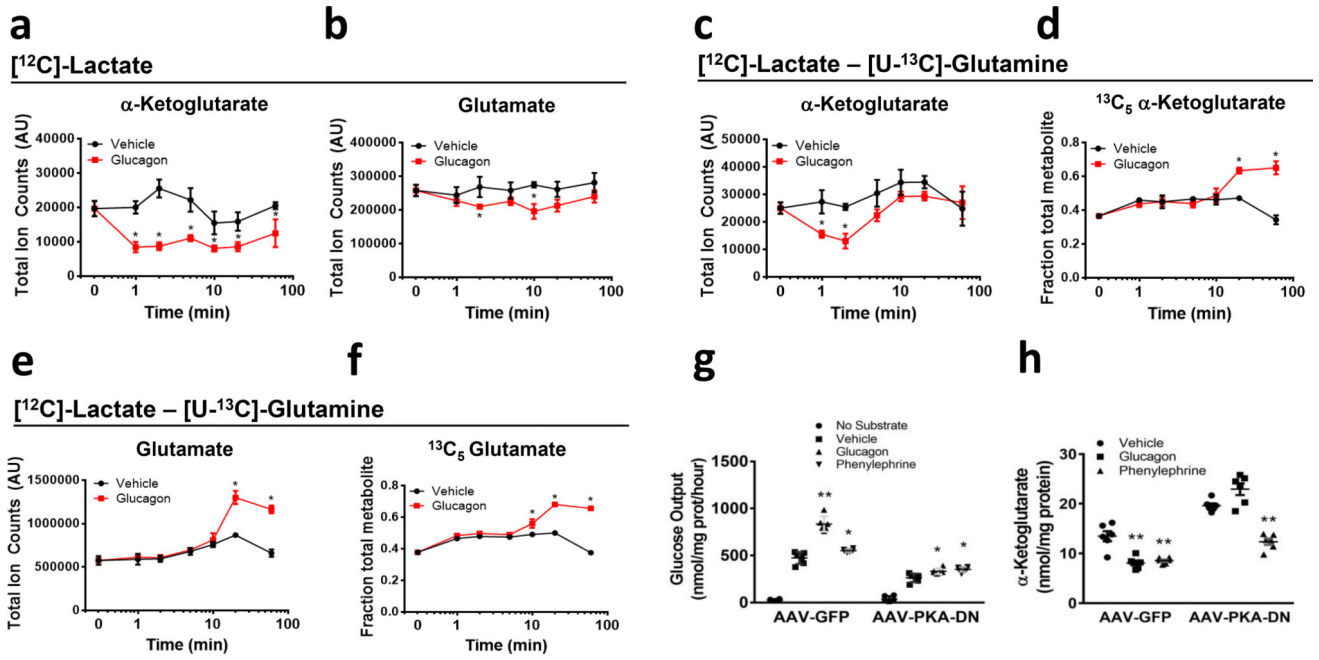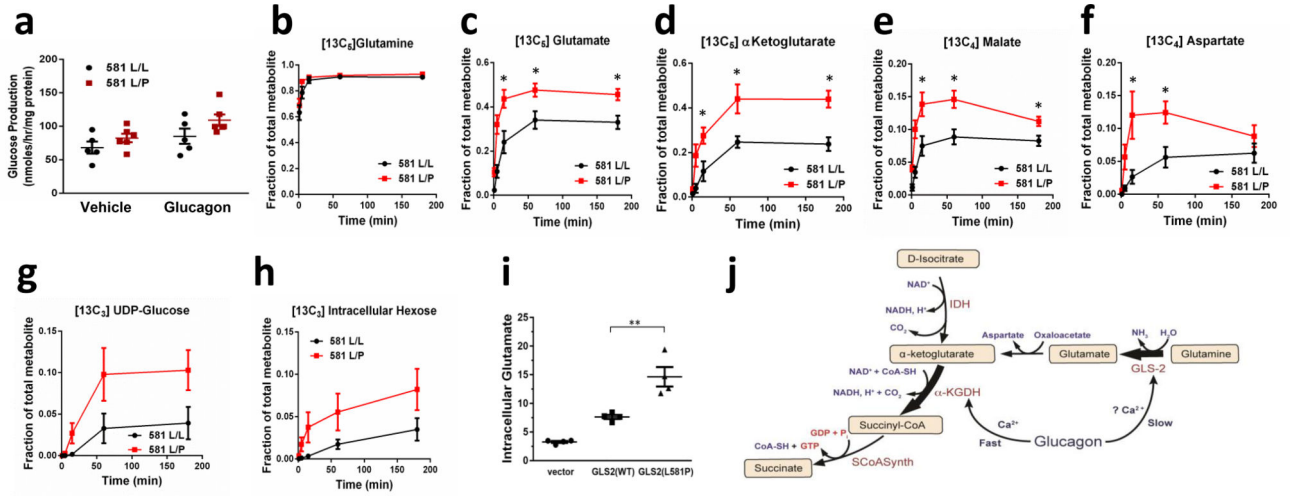
Figure 2.
Kinetics effects of glucagon on α-ketoglutarate and glutamate in primary hepatocytes (**a–f**). α-ketoglutarate and glutamate levels when (**a–b**) only [^{12}C]lactate was provided as substrate or (**c–d**) when both [^{12}C]lactate and [U-^{13}C]glutamine as substrates. (**e–f**) [5-^{13}C]α-ketoglutarate and [5-^{13}C]glutamate fraction of total metabolite when both [^{12}C]lactate and [U-^{13}C]glutamine were present as extracellular substrates. Values represent triplicates from a pool of hepatocytes from 4 mice and are the mean ± SEM. This experiment was performed once but the effect on α-ketoglutarate was repeated more than 5 times. Glucose production (**g**) and enzymatic measurement of α-ketoglutarate (**h**) in primary hepatocytes from mice previously infected with AAV-TBG-GFP or AAV-TBG-PKA-DN. *$P < 0.05$, **$P < 0.01$, two-tailed Student's *t*-test.

Figure 3.
In vivo glutamine and glucagon infusion study from mice infected with AAV-GFP or AAV-GLS2-sh (**a–e**). (**a**) Western blot from liver tissue of GLS2, phosphorylated and total Insulin Receptor β (IRβ), phosphorylated and total Akt, and GAPDH. Hepatic $[^{13}C_3]$glucose (**b**) and $[^{13}C_3]$glycerol (**c**) normalized to the tissue $[^{13}C_5]$-glutamine fraction. Blood glucose (**d**) and plasma insulin (**e**) measured following infusion. In all panels, values represent the mean of at least 5 biological replicates. These experiments were performed once. (**f**) Glucose production from primary hepatocytes from fasted GLS2-WT or GLS2-KO mice with indicated substrates: 1mM glutamine and/or 1mM lactate+0.1mM pyruvate in the presence or absence of 100nM glucagon for 1 hour. Values represent three biological replicates. (**g–m**). GLS2-WT and GLS2-KO mice were fed a chow diet. Animals were were evaluated for (**g**) fed and fasted blood glucose, (**h**) fasted plasma glucagon, (**i**) fasted plasma glutamine, and (**j**) fasted plasma insulin. WT: KO=13:25 (**k**) Representative immunofluorescence of glucagon (red) and insulin (green) stains in pancreatic islets of mice fasted overnight, merged with DAPI (blue). Scale bar represents 30 μm. **l**. Quantification of glucagon positive mass per islets from mice fasted overnight. WT: KO=10:9. **m**. Quantification of insulin positive surface area per islets from mice fasted overnight. (**n–q**). GLS2-WT and GLS2-KO mice were fed a high fat diet for 17 weeks. Animals were evaluated for (**n**) fasted blood glucose, (**o**) body weight, (**p**) fasted plasma glucagon, and (**q**) fasted plasma insulin. Throughout, data are mean ± SEM. *$P < 0.05$, two-tailed Student's t-test. NS, not significant.

Figure 4.
Glutamine metabolism in primary cryopreserved human hepatocytes from donors genotyped to be homozygous GLS L581L/L and heterozygous L581L/P. (**a**) Glucose production in the presence of glucagon or PBS vehicle for 1 hour with extracellular glutamine, lactate, and pyruvate substrates. Values are from 5 (L581L/L) and 6 (L581L/P) donors, each representing the mean of 3 technical replicates. *$P < 0.05$, by two way anova. **b–h**. Hepatocytes from GLS L581L/L and L581L/P donors were given [$^{13}C_5$]glutamine and unlabeled lactate and pyruvate in kinetic flux studies. Intracellular (**b**) [$^{13}C_5$]glutamine, (**c**) [$^{13}C_5$]glutamate, (**d**) [$^{13}C_5$]a-ketoglutarate, (**e**) [$^{13}C_4$]malate, (**f**) [$^{13}C_4$]aspartate, (**g**) [$^{13}C_6$]UDP-glucose, and (**h**) [$^{13}C_6$] hexose was measured. Values represent the mean of 6 biological replicates, each from a unique biological hepatocyte donor, for each group and time point, with each biological replicate representative of 3 technical replicates. Error bars represent SEM. The steady state (3 hour time point) data from this experiment was replicated in a separate study (data not shown). *$P < 0.05$, two-tailed Student's t-test. (**i**) Intracellular glutamate level was measured in immortalized human hepatocytes expressing either GLS2(WT) or GLS2(L581P), with cells transduced with lentivirus empty vector as a control. Values represent 4 biological replicates. **$P < 0.01$, two-tailed Student's t-test. (**j**) A model summarizing the proposed effects of glucagon on mitochondrial fluxes. IDH: isocitrate dehydrogenase; SCoASynth: succinate-CoA synthetase.